

## ARTICLE OPEN ACCESS

# A Multiple-Model-Informed Drug-Development Approach for Optimal Regimen Selection of an Oncolytic Virus in Combination With Pembrolizumab

Akihiro Yamada<sup>1</sup>  | Mary P. Choules<sup>2</sup>  | Frances A. Brightman<sup>3</sup>  | Shigeru Takeshita<sup>1</sup> | Shinsuke Nakao<sup>1</sup>  | Nobuaki Amino<sup>1</sup> | Takeshi Nakayama<sup>1</sup> | Masato Takeuchi<sup>1</sup> | Kanji Komatsu<sup>1</sup> | Fernando Ortega<sup>3</sup> | Hitesh Mistry<sup>3</sup>  | David Orrell<sup>3</sup> | Christophe Chassagnole<sup>3</sup>  | Peter L. Bonate<sup>2</sup>

<sup>1</sup>Astellas Pharma Inc., Tokyo, Japan | <sup>2</sup>Astellas Pharma Inc., Northbrook, Illinois, USA | <sup>3</sup>Physiomics Plc, Abingdon, UK

**Correspondence:** Akihiro Yamada ([akihiro.yamada@astellas.com](mailto:akihiro.yamada@astellas.com))

**Received:** 26 April 2024 | **Revised:** 18 November 2024 | **Accepted:** 9 December 2024

**Funding:** This study was funded by Astellas Pharma Inc., who contracted with Physiomics for this work.

## ABSTRACT

The antitumor efficacy of an intratumoral injection of a genetically engineered oncolytic vaccinia virus carrying human IL-7 and murine IL-12 genes (hIL-7/mIL-12-VV) was demonstrated in *CT26.WT*-bearing mice. In the *CT26.WT*-bearing mouse model, the efficacy of the combination of hIL-7/mIL-12-VV plus the anti-programmed cell death protein (PD)-1 antibody was determined to be correlated with the timing of administration: greater efficacy was observed when hIL-7/mIL-12-VV was administered before the anti-PD-1 agent instead of simultaneous administration. To identify an optimal dosing regimen for first-in-human clinical trials, a multiple model-informed drug-development (MIDD) approach was used through development of a quantitative systems pharmacology (QSP) model and an agent-based model (ABM). All models were built and verified using available literature and preclinical study data. Multiple dosing scenarios were explored using virtual populations by altering the interval between hIL-7/hIL-12-VV and pembrolizumab administration. In contrast with observations from preclinical studies, both the QSP and the ABM models demonstrated no antagonistic effect on the dose-dependent antitumor efficacy of hIL-7/hIL-12-VV by pembrolizumab in simulations of clinical therapy. Based on the MIDD strategy, it was recommended that the highest dose of hIL-7/hIL-12-VV and pembrolizumab should be administered on the same day, but with pembrolizumab administration following hIL-7/hIL-12-VV administration. Multiple different modeling approaches uniquely supported and informed the first-in-human clinical trial design by guiding the optimal dose and regimen selection.

## 1 | Introduction

In recent years, the field of cancer immunotherapy has revolutionized oncology by harnessing the body's immune system to recognize and eradicate tumors. However, designing effective immunotherapies and optimizing treatment strategies in this complex and dynamic field presents significant challenges. To address these challenges, quantitative systems pharmacology (QSP) modeling and/or agent-based modeling (ABM) have emerged as powerful tools for understanding and predicting the behavior of immuno-oncology systems [1].

QSP modeling is an interdisciplinary approach that combines mechanistic modeling, computational techniques, and experimental data to gain insights into the complex interactions between drugs, disease processes, and the human body [2]. In the application to clinical pharmacology and more specifically immuno-oncology, QSP models aim to capture the intricate dynamics of the immune system and tumor microenvironment, as well as the effects of immunotherapeutic agents such as immune checkpoint blockers (ICBs), chimeric antigen receptor T-cell (CAR-T) treatments, and bispecific antibody therapies [3–5].

This is an open access article under the terms of the [Creative Commons Attribution-NonCommercial-NoDerivs](https://creativecommons.org/licenses/by-nc-nd/4.0/) License, which permits use and distribution in any medium, provided the original work is properly cited, the use is non-commercial and no modifications or adaptations are made.

© 2025 The Author(s). *CPT: Pharmacometrics & Systems Pharmacology* published by Wiley Periodicals LLC on behalf of American Society for Clinical Pharmacology and Therapeutics.

## Summary

- What is the current knowledge on the topic?
  - Oncolytic viruses (OVs) have the potential to sensitize tumors to immune checkpoint blockade, potentially increasing patient response rate. The combination of an OV with an immune checkpoint blocker is currently being studied in clinical trials using a sequential administration strategy. However, their interaction potential is not fully understood and has not been investigated quantitatively by mechanistic modeling.
- What question did this study address?
  - The present study explores quantitatively the potential for interaction between an immune checkpoint blocker and an OV, with specific focus on the administration schedule of the 2 agents in relation to each other. The study helps to explain differences between the preclinical and clinical assessments.
- What does this study add to our knowledge?
  - This study provides a strategy for selection of an optimal clinical study design for the dosing of an OV followed by an immune checkpoint blocker, based on multiple MIDD.
- How might this change drug discovery, development, and/or therapeutics?
  - The present study highlighted the uncertainty of translating a dosing schedule from preclinical animal studies to first-in-human administration. In addition, it presented a multiple modeling approach to understand the complex biology involved with OV administration. The outcomes were used to support a clinical study design.

Conversely, ABM focuses on the behavior, interaction, and fate of entities represented in the model over time at the individual level using fundamental rules that govern the system [6]. Owing to the computational burden, ABMs typically represent a singular level within a more complex system and are subsequently linked to other modeling techniques (ODE-based) to fully represent the larger system. In the context of immunology, agents can represent various components, including immune cells, tumor cells, cytokines, and therapeutic agents [7]. The “Virtual Tumour” (VT) platform model, developed by Physiomics (Abingdon, UK), is an ABM of a growing tumor-cell population. This model aims to integrate and reproduce the effects that antitumor drugs, or radiotherapy, have on tumor cell-cycle progression and survival by reproducing the observed pharmacokinetic (PK) exposures and pharmacodynamic effects [8]. The VT model can predict how a tumor will respond to drug exposure and has been used previously for optimizing the dosing and scheduling of dual immuno-oncology combinations [9, 10].

Oncolytic viruses (OVs) are viruses that can disseminate in cancer cells and have emerged as a promising class of anticancer agents [11]. These genetically modified or naturally occurring viruses are designed to selectively destroy cancer cells, while leaving healthy cells unharmed [12]. More importantly, OVs possess unique immunomodulatory properties that can augment the antitumor immune response. By inducing immunogenic cell

death, promoting tumor antigen release, and modulating the tumor microenvironment, OVs have the potential to sensitize tumors to immune checkpoint blockade [13].

Immune checkpoint blockade is one of the most successful immunotherapy treatments. Tumor cells expressing programmed death-ligand (PD-L)1 on their surface and with a lymphocytic infiltrate, including melanoma, Hodgkin lymphoma, non-small cell lung, bladder, gastric, renal, and ovarian cancers, have been shown to respond well to anti-PD-1 therapy [14]. Among the responsive cancer types, although pembrolizumab or nivolumab was effective in about 30%–40% of patients with melanoma [15–18], the response rate in patients with advanced non-small cell lung cancer was about 15%–19% [19, 20]. Moreover, anti-PD-1 and anti-PD-L1 therapies showed a particularly low response rate in “cold tumors” such as pancreatic cancer [21]. Therefore, expanding the successful application of immune checkpoint blockade through combination therapy could have a marked impact on treatment effectiveness.

Immune checkpoint blockade can also inhibit viral replication through an increase in antiviral immunity and viral clearance [22, 23]. This action was demonstrated when an OV was combined with an anti-CTLA-4 antibody in Renca and MC38 tumor models, where the therapeutic benefit was found to be dependent on the timing of the 2 agents, with some schedules even producing antagonistic effects [23]. Similar timing dependence was observed in another mouse study combining an oncolytic vaccinia virus (OVV) with both anti-CTLA4 and anti-PD-1 antibodies [24]. Hence, the exact administration schedule of an OV and an ICB could be critical for efficacy. It has been suggested that an initial period of viral replication and direct targeting of the tumor before introducing an ICB is required for achieving the optimal therapeutic outcome [23]. Several clinical trials have explored the combination using a sequential administration strategy with varying dosing intervals (e.g., 1–6 weeks) [25–29]. However, there has been no clear evidence that immune activation by immune checkpoint blockade decreases antitumor efficacy of OVs. Interspecies differences between animal and human PK profiles are well known, and the implementation of an optimal dosing regimen determined by an animal model is not always translatable in designing a human clinical study.

Translational predictions based only on preclinical experimental data have high uncertainty due to interspecies differences in biology and kinetics. Modeling and simulation are tools for gaining insight into the complexities demonstrated by such combination therapies and can be utilized to optimize scheduling, while taking interspecies differences into account. The application of multiple modeling techniques within a model-informed drug-development (MIDD) approach increases confidence in model-based recommendations for optimal dosing schedules. In the present study, the observed interaction between a tumor-selective OVV encoding human IL-7 and murine IL-12, and an anti-PD-1 antibody was analyzed in preclinical experiments. The interaction was then predicted in humans by independent modelers through 2 different modeling approaches: QSP modeling and ABM.

The results were then compared to identify any consistencies or discrepancies between model conclusions. By comparing

the predictions from multiple modeling approaches, we can reinforce our confidence in the model-predicted dosing regimen when exploring the combination of a tumor-selective OVV and pembrolizumab in human clinical studies.

## 2 | Methods

### 2.1 | Mouse QSP Modeling

The combined effects of oncolytic adenoviruses and T-cell-mediated oncolysis in a murine tumor model were previously investigated using a semi-mechanistic QSP model [30]. Another semi-mechanistic QSP model, which includes key elements of the cancer immunity cycle, the tumor microenvironment, tumor growth, and dose-exposure-target modulation features, was developed to reproduce experimental data of CT26 tumor-size dynamics in mice upon administration of radiotherapy and/or a pharmacological immuno-oncology treatment such as an anti-PD-L1 agent [31]. By combining these models, a semi-mechanistic QSP mouse model that could explain the combination effects of OV and anti-PD-1 antibody was developed. A diagram of the combined model is shown in Figure 1.

Four independent preclinical experiments in *CT26.WT*-bearing mice (Exp1—Exp4) were used to inform a preclinical QSP model that describes the tumor volume dynamics in response to intratumorally administered hIL-7/mIL-12-VV

and/or anti-PD-1 antibody. For a detailed description of the preclinical experiments, see Supporting Information, including Methods S1, Table S1, and Figure S1. The measured tumor volumes were converted to tumor cell counts assuming  $10^6$  cells/mm<sup>3</sup> [30]. Parameters specific to hIL-7/mIL-12-VV (viral production size, infection rate, infected lysis rate, and virus elimination rate), immune stimulation by IL-7 and IL-12, and the tumor-growth rate constant for each experiment were optimized in NONMEM version 7.5 (ICON Development Solutions, Ellicott City, MD). In the analysis of combination therapy of hIL-7/mIL-12-VV and anti-PD-1 antibody, the antagonistic effect of the anti-PD-1 antibody was incorporated hypothetically as direct enhancement of virus clearance by the anti-PD-1 antibody. The ordinary differential equations used for the semi-mechanistic QSP model for mouse are presented in Supporting Information.

### 2.2 | Human QSP Model Simulations

Several QSP models representing checkpoint blocker combination therapies in the clinical setting have been proposed [3, 32, 33]. In this analysis, the most recent QSP model was selected, as its mechanistic description was considered the most appropriate [33]. The reported QSP model was modified in SimBiology, version 6.4.1 (Mathworks, Natick, MA) by incorporating OV and cancer cell infection components. The model structure was the same as in the preclinical semi-mechanistic QSP model, with some preclinical

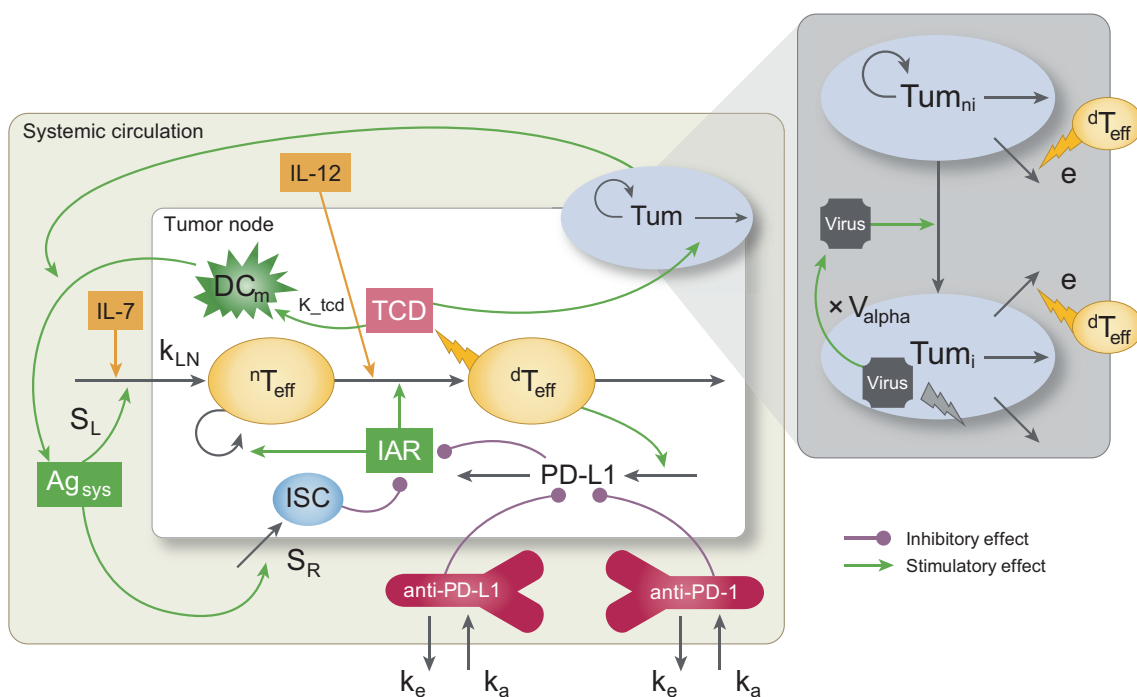


**FIGURE 1** | Schematic diagram of mouse QSP model.  $Ag_{sys}$ , a systemic level of tumor antigen presentation;  $DC_m$ , matured dendritic cells;  $dT_{eff}$ , cytotoxic effector T lymphocytes;  $e$ , rate of tumor-cell kill by differentiated effector T cells; IAR, immune activation rate; IL-7, interleukin 7; IL-12, interleukin 12; ISC, immune suppressive cells;  $k_a$ , absorption rate constant of anti-PD-1 antibody from depot compartment;  $k_e$ , elimination rate constant of anti-PD-1 antibody;  $k_{LN}$ , maximum influx rate of nondifferentiated precursors of cytotoxic effector T lymphocytes;  $K_{tcd}$ , sensitivity of  $DC_m$  to TCD value;  $nT_{eff}$ , nondifferentiated precursors of  $dT_{eff}$ ; PD-1, programmed cell death protein 1; PD-L1, programmed death-ligand 1; QSP, quantitative systems pharmacology;  $S_L$ , T-cell ability to infiltrate tumor tissue under systemic antigen exposure;  $S_R$ , sensitivity of cellular immunosuppression to accumulation of systemic antigen level; TCD, tumor-cell death;  $T_{eff}$ , effector T cells;  $T_{reg}$ , regulatory T cells; Tum, tumor cells;  $Tum_i$ , infected tumor cells;  $Tum_{ni}$ , noninfected tumor cells;  $V_{alpha}$ , viral production size.

parameters further optimized for the present model application. A diagram of the clinical QSP model is shown in Figure 2. The human QSP model represented only the tumor where hIL-7/hIL-12-VV, which carries human IL-12 instead of murine IL-12, was injected. The equations and parameters used for the clinical QSP model are listed in Tables S2–S5.

It was expected that hIL-7/hIL-12-VV would be administered at a fixed concentration (pfu/mL), and that the volume of the dose would be adjusted based on tumor size (longest dimension) anticipating consistent virus concentration across tumor size, to form 4 treatment groups:

1. 1.0 mL for tumor size  $\geq 1.0$  to  $< 2.0$  cm
2. 2.0 mL for tumor size  $\geq 2.0$  to  $< 3.0$  cm
3. 4.0 mL for tumor size  $\geq 3.0$  to  $< 4.0$  cm
4. 6.0 mL for tumor size  $\geq 4.0$  to  $\leq 4.5$  cm

Tumor-growth inhibition was investigated by simulation using the mechanistic QSP model for humans. All simulations were performed with MATLAB, version 2020a and 2023a (Mathworks, Natick, MA, USA). At first, a set of parameters for 125 virtual patients was generated, including a unique baseline tumor size between 1.0 cm and 4.5 cm for each patient in a uniform distribution manner. The initial cancer cell number was set as  $10^6$  cells, and then simulation was performed without any treatment up to 8000 days, to identify the time for each patient when the tumor grew to the designated baseline tumor size. If the tumor failed

to reach the designated size, the patient was eliminated from the virtual population. The values in each node at the time when the tumor reached the designated tumor size were extracted and substituted as initial conditions for each patient. The final simulation was then performed for each patient in each treatment group for up to 400 days.

The dose-dependent antitumor effect of hIL-7/hIL-12-VV was simulated at  $1 \times 10^7$  pfu/mL,  $1 \times 10^8$  pfu/mL, and  $5 \times 10^8$  pfu/mL. hIL-7/hIL-12-VV was administered intratumorally every 2 weeks. The antitumor effect of hIL-7/hIL-12-VV at  $5 \times 10^8$  pfu/mL in combination with pembrolizumab (400 mg, administered once every 6 weeks, starting from day 1, day 8, day 15, or day 29) was simulated to test the combination treatment effect.

The simulated time course of the change in tumor volume from baseline and the change in tumor diameter from baseline at 365 days were analyzed visually. The objective response rate (ORR) was calculated as the percentage of patients with 30% or more reduction in tumor diameter, corresponding to the complete response and partial response, based on Response Evaluation Criteria in Solid Tumors (RECIST). Based on simulated tumor volume-time course and ORR, an optimal regimen was proposed.

### 2.3 | Mouse ABM Modeling

A schematic diagram of the ABM is shown in Figure 3. The development of a VT model for treatment of CT26.WT-bearing

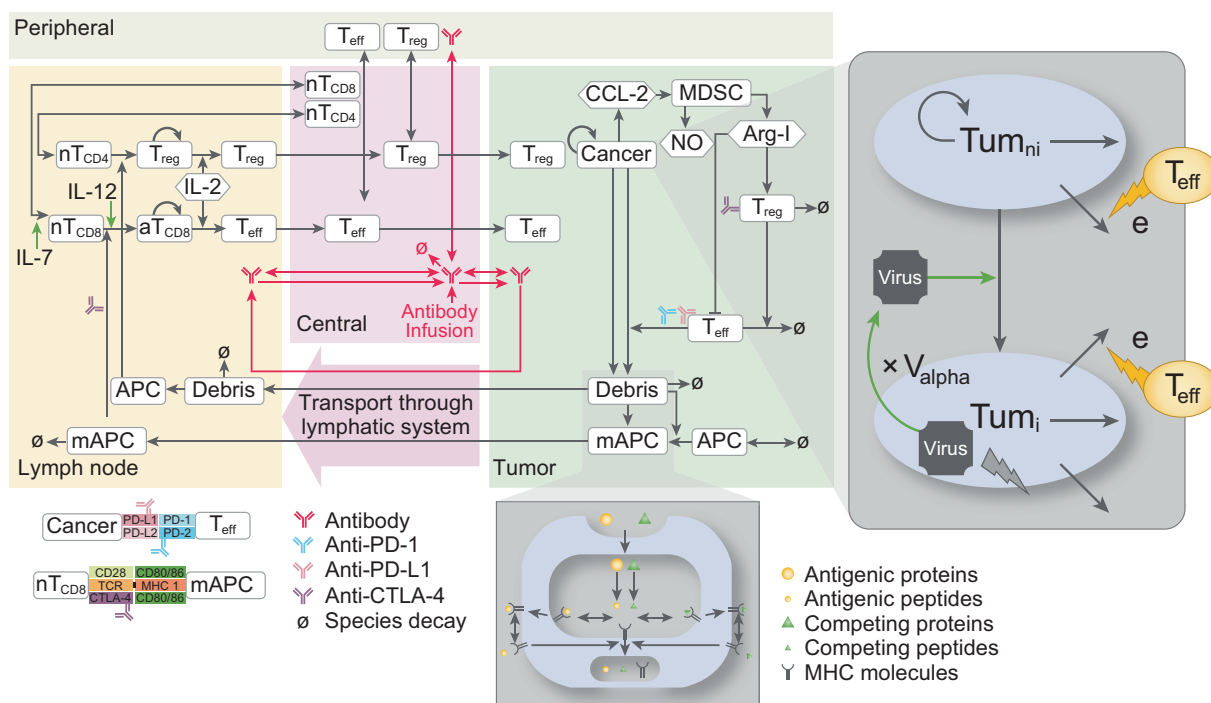


**FIGURE 2** | Schematic diagram of human QSP model. Human QSP model was built by combining the reported model of Wang et al. [33] and a portion of oncolytic virus mechanism of action in the preclinical QSP model shown in Figure 1. APC, antigen-presenting cell; Arg-1, arginase 1; aT<sub>CD8</sub>, activated CD8-positive T cells; CCL-2, chemokine (C-C motif) ligand 2; CTLA-4, cytotoxic T-lymphocyte-associated protein 4; e, rate of tumor-cell kill by differentiated effector T cells; IL-2, interleukin 2; IL-7, interleukin 7; IL-12, interleukin 12; mAPC, MHC-presenting APC; MDSC, myeloid-derived suppressor cells; MHC, major histocompatibility complex; nT<sub>CD4</sub>, naïve CD4-positive T cells; nT<sub>CD8</sub>, naïve CD8-positive T cells; NO, nitric oxide; PD-1, programmed cell death protein 1; PD-L1, programmed death-ligand 1; QSP, quantitative systems pharmacology; TCR, T-cell receptor; T<sub>eff</sub>, effector T cells; T<sub>reg</sub>, regulatory T cells; Tum<sub>i</sub>, infected tumor cells; Tum<sub>ni</sub>, noninfected tumor cells; V<sub>alpha</sub>, viral production size.

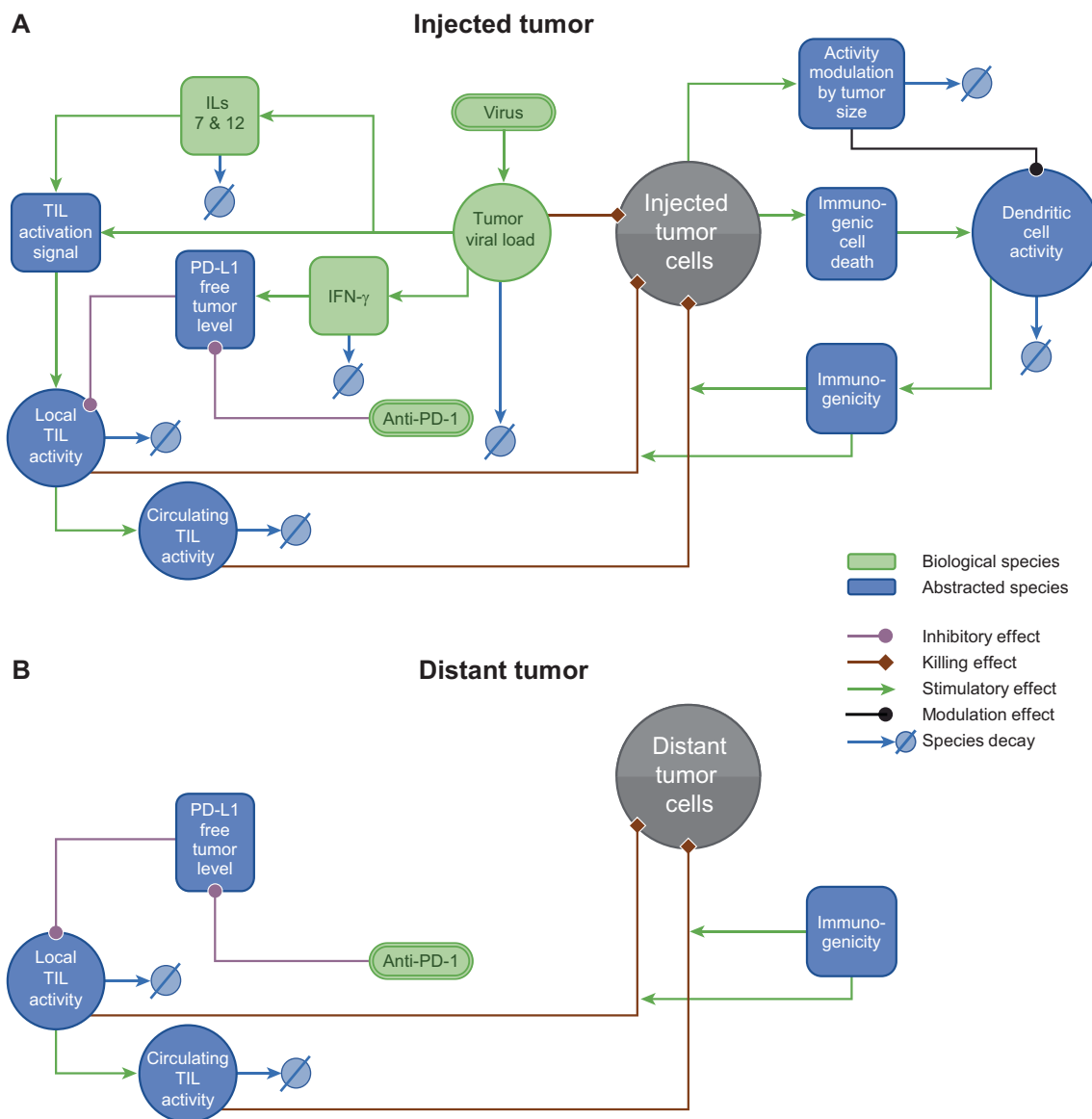


**FIGURE 3** | Schematic of the ABM VT model integrating the effects of combination therapy with hIL-7/mIL-12-VV and anti-PD-1 therapy at injected tumor (A) and distant tumor (B). Physiomics' model database references: PYC-MA-27, 29 (preclinical calibration) and PYC-MA-26, 28 (clinical calibration). ABM, agent-based model; IFN $\gamma$ , interferon  $\gamma$ ; hIL-7/mIL-12-VV, vaccinia virus carrying human IL-7 and murine IL-12 genes; IL-7, interleukin 7; IL-12, interleukin 12; PD-1, programmed cell death protein 1; PD-L1, programmed death-ligand 1; TIL, tumor-infiltrating lymphocyte; VT, Virtual Tumour model developed by Physiomics.

mouse with hIL-7/mIL-12-VV was conducted using a stepwise process. The model structure was informed by a range of literature sources [34–40], while the model parameters were calibrated against various data sets corresponding to experimental work reported by Nakao et al. [41] First, the baseline growth dynamics of the CT26.WT-bearing mice were calibrated against experimental data from control (untreated) tumors, the cell doubling time being adjusted to fit the mean tumor-growth time course.

Calibration of the pharmacodynamic effects of hIL-7/mIL-12-VV began with the simplest case of the unmodified virus alone (control OVV) in CT26.WT tumors. The direct oncolytic effect of the virus, the resulting induction of an adaptive immune response, and lysis of tumor cells by activated tumor-infiltrating lymphocytes (TILs) were all calibrated by fitting the corresponding model parameters to the mean tumor-growth time course

for tumors treated with OVV ( $4 \times 10^7$  pfu, on days 1, 3, and 5). Next, the dose–response for induction of IL-7, IL-12, and IFN- $\gamma$  by hIL-7/mIL-12-VV was calibrated, by fitting the model to data describing the increase in levels of these cytokines 24 h after treatment with single low ( $4 \times 10^5$  pfu), medium ( $4 \times 10^6$  pfu), or high ( $4 \times 10^7$  pfu) dose of hIL-7/mIL-12-VV. The dose response in terms of tumor-growth inhibition was also calibrated, by refining the values of parameters that determine TIL activation in response to interleukin production, and the interaction of the various stimulatory (direct and indirect TIL activation, immunogenic cell death, dendritic cell maturation, and immunogenicity), and inhibitory (PD-L1 upregulation and inhibition of TILs) factors. This was achieved by fitting the model parameters to the mean tumor-growth time course for animals treated with low, medium, or high doses of hIL-7/mIL-12-VV (on days 1, 3, and 5). Having defined a suitable set of parameters to represent the

actions of hIL-7/mIL-12-VV in injected tumors across a range of experimental studies, the effect on noninjected (distant) tumors was then calibrated by fitting the model in parallel to the mean tumor-growth time courses of injected and distant tumors (responders only) treated with hIL-7/mIL-12-VV ( $2 \times 10^7$  pfu, on days 1, 3, and 6). Finally, having established a consensus set of parameter values that allowed the model to capture the mechanism of action of hIL-7/mIL-12-VV across a range of data sets, in both injected and distant tumors, the model was calibrated for the effects of the anti-PD-1 antibody (DX400, the murine surrogate for pembrolizumab, at  $100 \mu\text{g}$  twice per week, starting on day 6), alone and in combination with hIL-7/mIL-12-VV ( $2 \times 10^7$  pfu, on days 1, 3, and 6), by simulating the PK profile of the antibody (from parameters given by Lindauer et al. in 2017 [42]) and fitting the model to the corresponding tumor-growth time-course data.

## 2.4 | Human ABM Model Simulations

Consideration of the exposure–response relationships for pembrolizumab in syngeneic mouse models [42] and human [43] shows that the 50% inhibitory concentration ( $IC_{50}$ ) of receptor occupancy in mouse and the clinical  $IC_{50}$  of interleukin (IL)-2 stimulation are comparable, suggesting that although the immune systems are certainly different between the 2 species, the concentration–response relationships for target engagement might be similar. Furthermore, no adequate experimental data were available to recalibrate the model taking differences between the mouse and human immune systems into account. Thus, for the clinical simulations, immune-system parameter values were retained from the mouse model. However, a clinical model PK for pembrolizumab [42] was substituted for pre-clinical PK, the tumor volume doubling time was adjusted to be 57 days [44], and initial tumor diameters of 10–20 mm and 5 mm were used for the injected and distant tumors, respectively, to reflect the slower growth and larger size of clinical tumors.

The dose-dependent antitumor effect of hIL-7/hIL-12-VV was simulated at  $1 \times 10^7$ ,  $1 \times 10^8$ , and  $5 \times 10^8$  pfu/mL. hIL-7/hIL-12-VV was administered intratumorally every 2 weeks. The antitumor effect of hIL-7/hIL-12-VV at  $1 \times 10^7$ ,  $1 \times 10^8$ , and  $5 \times 10^8$  pfu/mL in combination with pembrolizumab (400 mg administered once every 6 weeks starting, from day 1, day 4, day 8, day 15, or day 29) was simulated to test the combination treatment effect.

The time course of the change in tumor diameter from baseline, in injected and distant tumors, was simulated for 84 days after the start of treatment. Based on these simulations, an optimal dosing regimen was proposed.

## 3 | Results

### 3.1 | Mouse QSP Modeling

The list of parameters optimized for the mouse QSP model is summarized in the Table S2. The model-estimated tumor-volume–time profile and observed median tumor-size profile are overlaid in Figure S2. The estimated parameter responsible for the interaction between anti-PD1 antibody and OV—enhanced

viral clearance—showed 13.9% enhancement. This outcome suggested that tumor-growth inhibition was sensitive to viral elimination from the system and that the presence of anti-PD1 antibody critically impacted efficacy; virus-mediated tumor-growth suppression in the absence of anti-PD1 antibody would explain administration-sequence-sensitive efficacy. The model-estimated tumor-volume–time profile demonstrated greater antitumor efficacy using a regimen of hIL-7/mIL-12-VV administration in advance of anti-PD-1 administration compared with simultaneous administration.

### 3.2 | Human QSP Model Simulations

Simulated injected tumor volume-time profiles in treatment groups given  $1 \times 10^7$ ,  $1 \times 10^8$ , and  $5 \times 10^8$  pfu/mL hIL-7/hIL-12-VV every 2 weeks and the corresponding waterfall plots for injected tumor diameter are presented in Figure S3. Tumor response increased with increasing dose as the simulated ORRs at  $1 \times 10^7$ ,  $1 \times 10^8$ , or  $5 \times 10^8$  pfu/mL were 0%, 2%, and 22%, respectively. Simulated injected tumor-volume–time profiles in combination therapy with pembrolizumab treatment, starting at 0, 1, 2, and 4 weeks after the start of hIL-7/hIL-12-VV treatment, and the corresponding waterfall plots for injected tumor diameter, are presented in Figure 4, indicated as H-0W, H-1W, H-2W, and H-4W, respectively. The simulated ORRs when pembrolizumab treatment started at 0, 1, 2, and 4 weeks after the start of hIL-7/hIL-12-VV treatment were all the same across doses at 48%. No obvious differences in any treatment regimen were observed. Simulated ORR at day 100 was 21% for pembrolizumab treatment starting at 0 weeks after the start of hIL-7/hIL-12-VV, 21% for 1 week, 19% for 2 weeks, and 15% for 4 weeks.

### 3.3 | Mouse ABM Modeling

The model developed for CT26.WT-bearing mice described well the observed data for baseline growth dynamics (Figures S4A, S5A,B), tumor dynamics with unmodified virus alone (Figure S4B), tumor dynamics with hIL-7/mIL-12-VV (Figures S4C, S5C), tumor dynamics of distant tumor (Figure S5B,D), tumor dynamics with anti-PD-1 antibody (Figure S5E,F), and tumor dynamics with combination therapy (Figure S5G,H).

### 3.4 | Human ABM Model Simulations

A consistent regression of the injected tumor was observed, while the response of the distant tumor was more strongly dose dependent (Figure S7). The combination responses for the 3 dose levels of hIL-7/hIL-12-VV with or without pembrolizumab, dosed according to 5 different schedules, are plotted in Figure 5. For all the treatment schedules, there was no significant difference in the size of the injected tumor at the 80-day endpoint. The results for the noninjected tumor were more differentiated by 80 days. For treatment with hIL-7/hIL-12-VV alone, the tumor showed progression at the lowest dose ( $1 \times 10^7$  pfu/mL), stasis at the intermediate dose ( $1 \times 10^8$  pfu/mL), and regression at the highest dose ( $5 \times 10^8$  pfu/mL), with the tumor shrinking to approximately 38% of the initial size. In combination with pembrolizumab, stasis of the noninjected tumor was observed consistently at the lowest dose of hIL-7/

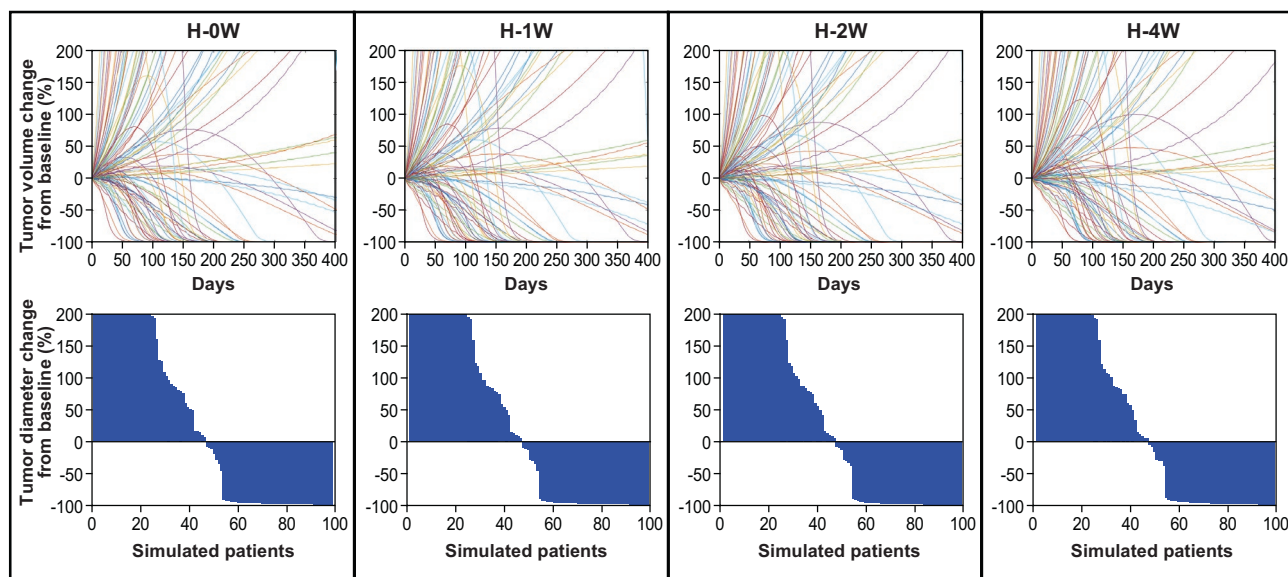


**FIGURE 4** | Predicted tumor volume-time profile (top) and waterfall plots (bottom) at dosing intervals of 0, 1, 2, and 4 weeks between hIL-7/hIL-12-VV and pembrolizumab administration to patients. hIL-7/hIL-12-VV was administered at high dose (H:  $5 \times 10^8$  pfu/mL) and pembrolizumab was administered at 400 mg once every 6 weeks. H, high dose; H-0W, 0 weeks between hIL-7/hIL-12-VV and pembrolizumab; H-1W, 1 week between hIL-7/hIL-12-VV and pembrolizumab; H-2W, 2 weeks between hIL-7/hIL-12-VV and pembrolizumab; H-4W, 4 weeks between hIL-7/hIL-12-VV and pembrolizumab; hIL-7/hIL-12-VV, vaccinia virus carrying human *IL-7* and *IL-12* genes; *IL-7*, interleukin 7; *IL-12*, interleukin 12.

hIL-12-VV. At the intermediate dose, the response showed some dependence on the dosing interval between hIL-7/hIL-12-VV and pembrolizumab: when pembrolizumab treatment was delayed as long as 4 weeks after hIL-7/hIL-12-VV treatment, the noninjected tumor shrank to around 50% of the initial size, compared with regression to around 30%–35% for shorter dosing intervals (0–2 weeks). This schedule dependence is not apparent at the highest dose, with all schedules resulting in regression of the tumor to around 20%–25% of the initial size.

#### 4 | Discussion

A multiple modeling approach was taken to inform the phase 1 first-in-human clinical study design for the dosing of an OV followed by an immune checkpoint blocker. Overall, both models (QSP and ABM) captured the observed preclinical data available. The preclinical semi-mechanistic QSP model demonstrated successfully the observed difference in efficacy following different treatment regimens. The model reproduced the preclinical data where higher efficacy was observed with sequential administration compared to simultaneous administration. More specifically, the model demonstrated greater tumor reduction at the injected tumor over the distant tumor (Figure S2). Although in the preclinical experimental studies, a difference in efficacy between treatment regimens was observed only at the distant tumor, the number of mice showing regrowth of the tumor at the injected site was larger following simultaneous administration, suggesting a weaker antagonistic effect might exist at the injected tumor, as well as at the distant tumor. Taking these observations into account, the preclinical QSP model might overestimate the antagonistic effect of ICBs at the injected tumor.

In the preclinical QSP model, the interaction of ICBs with OV was represented as the enhancement of the clearance of

OV—assumed to result from antiviral antibodies generated via stimulated immunity, which corresponds to the enhancement of virus elimination rate constant. Conversely, the observed regimen-sensitive tumor-growth inhibition of the combination therapy might be numerically explained as the presence of ICBs simultaneously enhancing the clearance rate of infected tumor cells and the clearance of OV in infected tumor cells, resulting in the elimination of OV from the system. However, from the available experimental data, tumor growth at the injected site was almost completely suppressed in OV monotherapy and, hence, the enhanced T-cell-mediated infected tumor-cell killing could not be identified. Regarding elimination of the virus from the system, the enhancement of viral clearance in infected cancer cells by activated cytotoxic lymphocytes and the enhancement of viral clearance by antiviral antibody would be considered synonymous and result in a similar outcome.

The preclinical ABM also captured successfully the range of data for hIL-7/mIL-12-VV and anti-PD-1 therapy, both as monotherapies and in combination. The model reproduced the combination effect of hIL-7/mIL-12-VV with anti-PD-1 antibody in injected and distant tumors in the *CT26.WT*-bearing mice.

Both preclinical models were then translated into human clinical models to carry out predictive simulations, focusing mainly on the impact of combination dose scheduling on efficacy. The reported clinical QSP model [33] was modified in SimBiology by incorporating OV and cancer cell infection components that had been used in the preclinical semi-mechanistic QSP model. Parameter translation was carefully considered to address the overestimation by the preclinical model. The modified QSP model for the clinical case study was used to simulate tumor-growth inhibition only at the injected tumor because the clinical

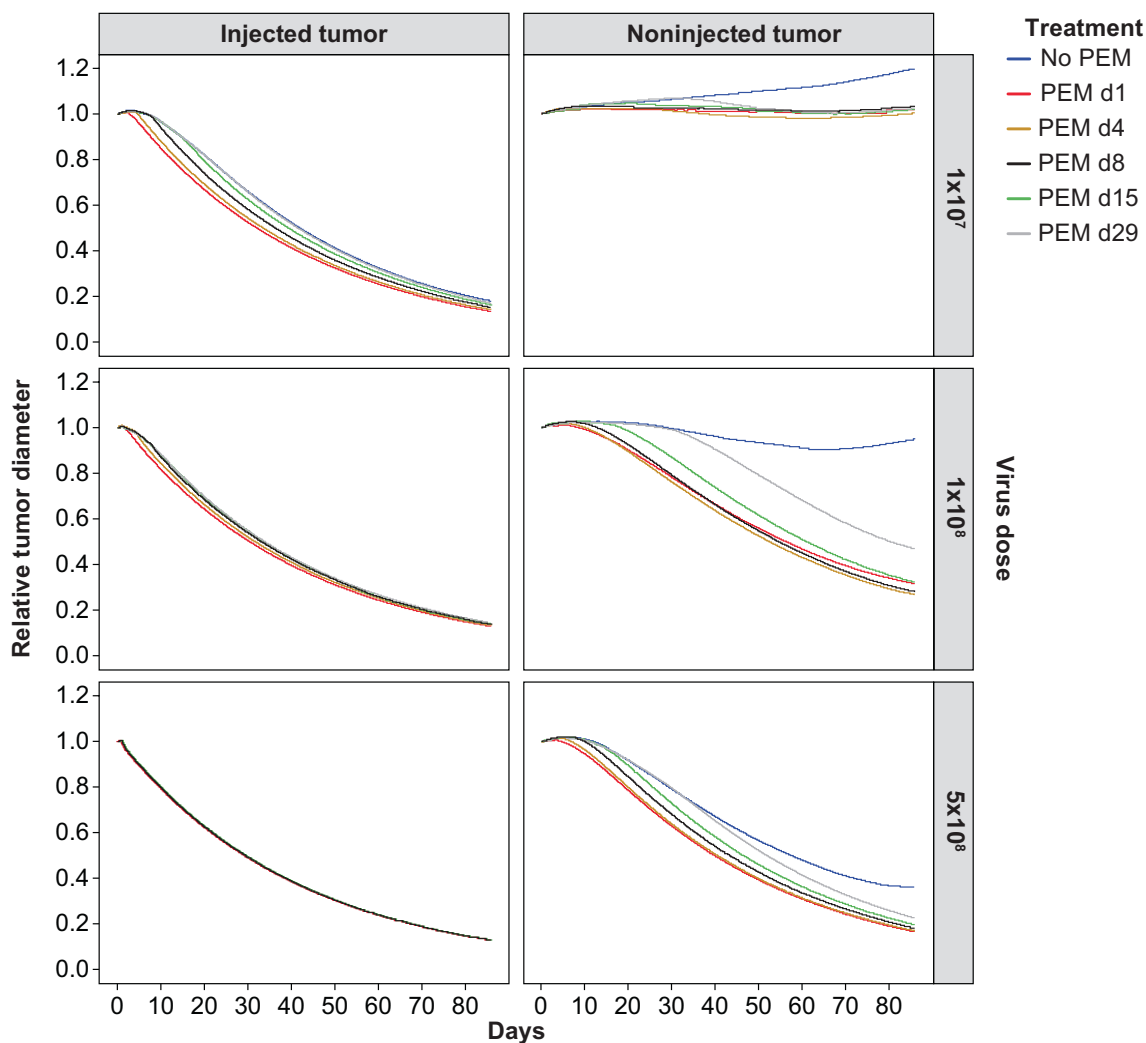


**FIGURE 5** | Predicted tumor diameter time-course profiles in the injected and noninjected (distant) tumor following administration of hIL-7/hIL-12-VV (top row  $1 \times 10^7$  pfu/mL, middle row  $1 \times 10^8$  pfu/mL, and bottom row  $5 \times 10^8$  pfu/mL, on days 1, 15, and 29) alone or in combination with pembrolizumab (400 mg once every 6 weeks, starting on day 1, 4, 8, 15, or 29) to patients. hIL-7/hIL-12-VV, vaccinia virus carrying human *IL-7* and *IL-12* genes; *IL-7*, interleukin 7; *IL-12*, interleukin 12; PEM, pembrolizumab. For reasons of clarity, prediction intervals have been omitted; predicted tumor diameter time-course profiles in the noninjected tumor following administration of hIL-7/hIL-12-VV ( $1 \times 10^8$  pfu/mL on days 1, 15, and 29) alone or in combination with pembrolizumab (400 mg once every 6 weeks, starting on day 1 or 29), showing corresponding 90% prediction intervals, are given in Figure S8.

QSP model had a single tumor compartment. As the simulations carried out using the preclinical QSP model demonstrated a regimen-dependent efficacy difference at both the injected and distant tumors, the clinical QSP model was considered more applicable for investigating antagonism between the anti-PD-1 antibody and hIL-7/hIL-12-VV. The preclinical ABM was translated to the clinical setting by substituting clinical PK for preclinical PK and adjusting the initial tumor size and doubling time to better reflect clinical tumor-growth dynamics.

Both translated clinical models demonstrated that tumor-growth inhibition by hIL-7/hIL-12-VV was dose dependent at the tested doses of  $1 \times 10^7$ ,  $1 \times 10^8$ , and  $5 \times 10^8$  pfu/mL. In the ABM, the dose-dependent effect was more apparent for distant tumors, with antitumor effect at the injected tumor appearing to be mostly saturated. The highest dose of  $5 \times 10^8$  pfu/mL was selected for the combination predictions used for the QSP model based on the recommended phase 2 dose. However, a range of doses was still explored using the ABM.

The tumor-growth-inhibition effect for a combination of hIL-7/hIL-12-VV and pembrolizumab was simulated with both models using administration intervals of 0, 1, 2, or 4 weeks between hIL-7/hIL-12-VV and the subsequent dosing of pembrolizumab. Based on the clinical QSP model, the ORR at 365 days after treatment and the tumor-growth-inhibition profiles demonstrated no obvious differences between the treatment schedules. The rank order for the best sequential combination based on the estimated ORR at 100 days after treatment was 1 week  $\geq$  0 week  $>$  2 weeks  $>$  4 weeks (Figure 4). Although no obvious differences were observed at later times, based on QSP model predictions, the regimen that might be expected to demonstrate the highest efficacy would be a 1-week interval between dosing of hIL-7/hIL-12-VV and pembrolizumab. Predictions demonstrated by the ABM agreed with the QSP model at both low ( $1 \times 10^7$  pfu/mL) and high ( $5 \times 10^8$  pfu/mL) doses of hIL-7/hIL-12-VV. At the intermediate dose ( $1 \times 10^8$  pfu/mL), there appeared to be greater sensitivity to scheduling, with pembrolizumab administration on

**TABLE 1** | A summary comparing clinical QSP model and clinical ABM.

	Clinical QSP model	Clinical ABM
Software	MATLAB, SimBiology	Virtual Tumour (coded in MATLAB)
Number of equations	160	67
Number of species	124	34
Number of parameters	185	47
Time to run	Approximately 2h	Around 90s per individual simulation (overall run time depends on the number of individual simulations required)
Output	No clear difference was observed. The rank order of efficacy for the interval of pembrolizumab administration after OV administration was 1 week > 0 week > 2 weeks > 4 weeks	No clear difference was observed. The rank order of efficacy for the interval of pembrolizumab administration after OV administration was 1 week > 0 week > 2 weeks > 4 weeks
Limitations	Only preclinical data available for calibration No clinical validation Simulation of injected tumor only	Only preclinical data available for calibration No clinical validation

Abbreviations: ABM, agent-based model; OV, oncolytic virus; QSP, quantitative systems pharmacology.

day 29 generating the weakest response in the distant tumor. However, there was no appreciable difference, especially by the end of the simulation period, between the responses for dosing of pembrolizumab with other offsets (with dosing starting on days 1, 4, 8, or 15). Based on the ABM, any sequential dosing where pembrolizumab is administered < 29 days following hIL-7/mIL-12-VV administration would be appropriate. Therefore, both models appeared to agree that combination scheduling (when the interval is  $\leq 14$  days) might not have a significant effect on tumor-growth inhibition.

The results from both models helped to inform the clinical study design. The schedule explored in the clinical study was hIL-7/mIL-12-VV injected directly into the tumor on day 1 and day 15 of two 28-day cycles. Patients in the combination cohort were given pembrolizumab on cycle 1 day 1, with subsequent infusions every 6 weeks. This study design was selected based on the results generated by both models, the administration schedule of pembrolizumab, the administration schedule of hIL-7/mIL-12-VV, and the burden on the clinical study site and the patients. Based on all factors involved, day 1 dosing was selected and remained in agreement with qualitative trend in the modeling results.

A summary comparing both models can be found in Table 1. Overall, although both models take a different approach to the present problem and resulted in similar outcomes, the degree of complexity, ease of development, and limitations of each model vary. A limitation of both models was that only preclinical experimental data were available for model calibration, hence model translation to clinical applications could not be validated. The omission of the distant tumor site was a specific limitation for the QSP model.

A key aspect to the appropriate application of modeling and simulation in drug-development and regulatory evaluation is ensuring model credibility [45]. With increasing application of MIDD approaches and the advances in computational analysis

techniques, it is important to consider all factors involved in model building and interpretation. Some of those factors may include: software; ease of development; model run duration; platform versatility; and output type [46, 47]. Applying multiple modeling approaches to a singular problem may offer confidence when the model outcomes are the same. However, it is possible that the model predictions will differ, leading to further uncertainty. In such cases, the result from a model with higher credibility, based on the degree of the uncertainty included in the model, or the possible impact on patient safety (risk-benefit analysis), should be prioritized.

In the present application, the MIDD approach resulted in agreement between the 2 modeling approaches. Although uncertainty remains from a quantitative perspective, the fact that both models suggested the same qualitative trend reinforces the MIDD recommendation for designing an optimal clinical regimen.

#### Author Contributions

A.Y., M.P.C., F.A.B., and P.L.B. wrote the manuscript. A.Y., M.P.C., F.A.B., S.T., S.N., N.A., K.K., F.O., H.M., D.O., C.C., and P.L.B. designed the research. A.Y., F.A.B., S.N., N.A., T.N., M.T., F.O., H.M., D.O., and C.C. performed the research. A.Y., M.P.C., F.A.B., S.T., K.K., F.O., H.M., D.O., C.C., and P.L.B. analyzed the data.

#### Acknowledgments

Editorial and creative support was provided by Oxford PharmaGenesis Inc., Newtown, PA, USA, which was funded by Astellas Pharma Inc., in accordance with Good Publication Practice (GPP) 2022 and International Committee of Medical Journal Editors (ICMJE) guidelines.

#### Conflicts of Interest

A.Y., S.T., S.N., N.A., T.N., M.T., and K.K. are employees of Astellas Pharma Inc., Tokyo, Japan, and may own stock or stock options in the

company. M.P.C. and P.L.B. are employees of Astellas Pharma Inc., Northbrook, IL, USA. F.A.B., F.O., H.M., D.O., and C.C. are, or were, employees of Physiomics plc, Abingdon, UK and may own stock or stock options in the company, and received funding from Astellas.

### Data Availability Statement

Researchers may request access to anonymized participant-level data, trial-level data, and protocols from Astellas-sponsored clinical trials at [www.clinicalstudydatarequest.com](http://www.clinicalstudydatarequest.com). For the Astellas criteria on data sharing see: <https://clinicalstudydatarequest.com/Study-Sponsors/Study-Sponsors-Astellas.aspx>.

### References

1. D. Valentinuzzi and R. Jeraj, "Computational Modelling of Modern Cancer Immunotherapy," *Physics in Medicine and Biology* 65 (2020): 24TR01.
2. I. Zineh, "Quantitative Systems Pharmacology: A Regulatory Perspective on Translation," *CPT: Pharmacometrics & Systems Pharmacology* 8 (2019): 336–339.
3. O. Milberg, C. Gong, M. Jafarnejad, et al., "A QSP Model for Predicting Clinical Responses to Monotherapy, Combination and Sequential Therapy Following CTLA-4, PD-1, and PD-L1 Checkpoint Blockade," *Scientific Reports* 9 (2019): 11286.
4. A. P. Singh, W. Chen, X. Zheng, et al., "Bench-To-Bedside Translation of Chimeric Antigen Receptor (CAR) T Cells Using a Multiscale Systems Pharmacokinetic-Pharmacodynamic Model: A Case Study With Anti-BCMA CAR-T," *CPT: Pharmacometrics & Systems Pharmacology* 10 (2021): 362–376.
5. J. Weddell, "Mechanistically Modeling Peripheral Cytokine Dynamics Following Bispecific Dosing in Solid Tumors," *CPT: Pharmacometrics & Systems Pharmacology* 12 (2023): 1726–1737.
6. V. T. Truong, P. G. Baverel, G. D. Lythe, P. Vicini, J. W. T. Yates, and V. F. S. Dubois, "Step-By-Step Comparison of Ordinary Differential Equation and Agent-Based Approaches to Pharmacokinetic-Pharmacodynamic Models," *CPT: Pharmacometrics & Systems Pharmacology* 11 (2022): 133–148.
7. A. Ruiz-Martinez, C. Gong, H. Wang, et al., "Simulations of Tumor Growth and Response to Immunotherapy by Coupling a Spatial Agent-Based Model With a Whole-Patient Quantitative Systems Pharmacology Model," *PLoS Computational Biology* 18 (2022): e1010254.
8. D. Orrell and E. Fernandez, "Using Predictive Mathematical Models to Optimise the Scheduling of Anti-Cancer Drugs," *Innovations in Pharmaceutical Technology* 33 (2010): 59–62.
9. F. Ortega, F. A. Brightman, and C. Chassagnole, "Optimizing Dual Immuno-Oncology Combinations With a Virtual Tumor [Abstract]," *Cancer Research* 80, no. 16 Suppl (2020): LB-392.
10. F. Brightman, F. Ortega, D. Orrell, and C. Chassagnole, "The Abscopal Effect: Modelling and Predicting the Effect of Radiation Therapy on Non-irradiated Tumour When Combined With Immune Checkpoint Blockers [Abstract]," *Cancer Research* 81, no. 13 Suppl (2021): 232.
11. P. Muthukutty and S. Y. Yoo, "Oncolytic Virus Engineering and Utilizations: Cancer Immunotherapy Perspective," *Viruses* 15 (2023): 1645.
12. T. C. Liu, E. Galanis, and D. Kirn, "Clinical Trial Results With Oncolytic Virotherapy: A Century of Promise, a Decade of Progress," *Nature Clinical Practice. Oncology* 4 (2007): 101–117.
13. C. Lovatt and A. L. Parker, "Oncolytic Viruses and Immune Checkpoint Inhibitors: The "Hot" New Power Couple," *Cancers* 15 (2023): 4178.
14. S. L. Topalian, C. G. Drake, and D. M. Pardoll, "Immune Checkpoint Blockade: A Common Denominator Approach to Cancer Therapy," *Cancer Cell* 27 (2015): 450–461.
15. O. Hamid, C. Robert, A. Daud, et al., "Safety and Tumor Responses With Lambrolizumab (Anti-PD-1) in Melanoma," *New England Journal of Medicine* 369 (2013): 134–144.
16. C. Robert, G. V. Long, B. Brady, et al., "Nivolumab in Previously Untreated Melanoma Without BRAF Mutation," *New England Journal of Medicine* 372 (2015): 320–330.
17. S. L. Topalian, M. Sznol, D. F. McDermott, et al., "Survival, Durable Tumor Remission, and Long-Term Safety in Patients With Advanced Melanoma Receiving Nivolumab," *Journal of Clinical Oncology* 32 (2014): 1020–1030.
18. C. Robert, A. Ribas, J. D. Wolchok, et al., "Anti-Programmed-Death-Receptor-1 Treatment With Pembrolizumab in Ipilimumab-Refractory Advanced Melanoma: A Randomised Dose-Comparison Cohort of a Phase 1 Trial," *Lancet* 384 (2014): 1109–1117.
19. N. A. Rizvi, J. Mazières, D. Planchard, et al., "Activity and Safety of Nivolumab, an Anti-PD-1 Immune Checkpoint Inhibitor, for Patients With Advanced, Refractory Squamous Non-small-Cell Lung Cancer (CheckMate 063): A Phase 2, Single-Arm Trial," *Lancet Oncology* 16 (2015): 257–265.
20. E. B. Garon, N. A. Rizvi, R. Hui, et al., "Pembrolizumab for the Treatment of Non-small-Cell Lung Cancer," *New England Journal of Medicine* 372 (2015): 2018–2028.
21. D. Kabacaoglu, K. J. Ciecieski, D. A. Ruess, and H. Algül, "Immune Checkpoint Inhibition for Pancreatic Ductal Adenocarcinoma: Current Limitations and Future Options," *Frontiers in Immunology* 9 (2018): 1878.
22. C. Y. Chen, B. Hutzen, M. F. Wedekind, and T. P. Cripe, "Oncolytic Virus and PD-1/PD-L1 Blockade Combination Therapy," *Oncolytic Virotherapy* 7 (2018): 65–77.
23. J. J. Rojas, P. Sampath, W. Hou, and S. H. Thorne, "Defining Effective Combinations of Immune Checkpoint Blockade and Oncolytic Virotherapy," *Clinical Cancer Research* 21 (2015): 5543–5551.
24. L. Fend, T. Yamazaki, C. Remy, et al., "Immune Checkpoint Blockade, Immunogenic Chemotherapy or IFN- $\alpha$  Blockade Boost the Local and Abscopal Effects of Oncolytic Virotherapy," *Cancer Research* 77 (2017): 4146–4157.
25. E. Massarelli, W. William, F. Johnson, et al., "Combining Immune Checkpoint Blockade and Tumor-Specific Vaccine for Patients With Incurable Human Papillomavirus 16-Related Cancer: A Phase 2 Clinical Trial," *JAMA Oncology* 5 (2019): 67–73.
26. I. Puzanov, M. M. Milhem, D. Minor, et al., "Talimogene Laherparepvec in Combination With Ipilimumab in Previously Untreated, Unresectable Stage IIIB-IV Melanoma," *Journal of Clinical Oncology* 34 (2016): 2619–2626.
27. J. Chesney, I. Puzanov, F. Collichio, et al., "Randomized, Open-Label Phase II Study Evaluating the Efficacy and Safety of Talimogene Laherparepvec in Combination With Ipilimumab Versus Ipilimumab Alone in Patients With Advanced, Unresectable Melanoma," *Journal of Clinical Oncology* 36 (2018): 1658–1667.
28. C. Monge, C. Xie, Y. Myojin, et al., "Phase I/II Study of PexaVec in Combination With Immune Checkpoint Inhibition in Refractory Metastatic Colorectal Cancer," *Journal for Immunotherapy of Cancer* 11 (2023): 11.
29. F. Nassiri, V. Patil, L. S. Yefet, et al., "Oncolytic DNX-2401 Virotherapy Plus Pembrolizumab in Recurrent Glioblastoma: A Phase 1/2 Trial," *Nature Medicine* 29 (2023): 1370–1378.
30. P. S. Kim, J. J. Crivelli, I. K. Choi, C. O. Yun, and J. R. Wares, "Quantitative Impact of Immunomodulation Versus Oncolysis With Cytokine-Expressing Virus Therapeutics," *Mathematical Biosciences and Engineering* 12 (2015): 841–858.
31. Y. Kosinsky, S. J. Dovedi, K. Peskov, et al., "Radiation and PD-(L)1 Treatment Combinations: Immune Response and Dose Optimization

via a Predictive Systems Model,” *Journal for Immunotherapy of Cancer* 6 (2018): 17.

32. H. Wang, R. J. Sové, M. Jafarnejad, et al., “Conducting a Virtual Clinical Trial in HER2-Negative Breast Cancer Using a Quantitative Systems Pharmacology Model With an Epigenetic Modulator and Immune Checkpoint Inhibitors,” *Frontiers in Bioengineering and Biotechnology* 8 (2020): 141.

33. H. Wang, H. Ma, R. J. Sové, L. A. Emens, and A. S. Popel, “Quantitative Systems Pharmacology Model Predictions for Efficacy of Atezolizumab and Nab-Paclitaxel in Triple-Negative Breast Cancer,” *Journal for Immunotherapy of Cancer* 9 (2021): e002100.

34. L. Zitvogel, L. Apetoh, F. Ghiringhelli, and G. Kroemer, “Immunological Aspects of Cancer Chemotherapy,” *Nature Reviews. Immunology* 8 (2008): 59–73.

35. K. M. Storey, S. E. Lawler, and T. L. Jackson, “Modeling Oncolytic Viral Therapy, Immune Checkpoint Inhibition, and the Complex Dynamics of Innate and Adaptive Immunity in Glioblastoma Treatment,” *Frontiers in Physiology* 11 (2020): 151.

36. M. E. Raeber, Y. Zurbuchen, D. Impellizzeri, and O. Boyman, “The Role of Cytokines in T-Cell Memory in Health and Disease,” *Immunological Reviews* 283 (2018): 176–193.

37. Z. P. Parra-Guillen, P. Berraondo, E. Grenier, B. Ribba, and I. F. Tronconiz, “Mathematical Model Approach to Describe Tumour Response in Mice After Vaccine Administration and Its Applicability to Immune-Stimulatory Cytokine-Based Strategies,” *AAPS Journal* 15 (2013): 797–807.

38. G. Kroemer, L. Galluzzi, O. Kepp, and L. Zitvogel, “Immunogenic Cell Death in Cancer Therapy,” *Annual Review of Immunology* 31 (2013): 51–72.

39. L. Galluzzi, A. Buqué, O. Kepp, L. Zitvogel, and G. Kroemer, “Immunogenic Cell Death in Cancer and Infectious Disease,” *Nature Reviews. Immunology* 17 (2017): 97–111.

40. A. G. Duffy and T. F. Greten, “Immunological Off-Target Effects of Standard Treatments in Gastrointestinal Cancers,” *Annals of Oncology* 25 (2014): 24–32.

41. S. Nakao, Y. Arai, M. Tasaki, et al., “Intratumoral Expression of IL-7 and IL-12 Using an Oncolytic Virus Increases Systemic Sensitivity to Immune Checkpoint Blockade,” *Science Translational Medicine* 12 (2020): 12.

42. A. Lindauer, C. R. Valiathan, K. Mehta, et al., “Translational Pharmacokinetic/Pharmacodynamic Modeling of Tumor Growth Inhibition Supports Dose-Range Selection of the Anti-PD-1 Antibody Pembrolizumab,” *CPT: Pharmacometrics & Systems Pharmacology* 6 (2017): 11–20.

43. A. Patnaik, S. P. Kang, D. Rasco, et al., “Phase I Study of Pembrolizumab (MK-3475; Anti-PD-1 Monoclonal Antibody) in Patients With Advanced Solid Tumors,” *Clinical Cancer Research* 21 (2015): 4286–4293.

44. P. M. Stell, “Time to Recurrence of Squamous Cell Carcinoma of the Head and Neck,” *Head & Neck* 13 (1991): 277–281.

45. C. Kuemmel, Y. Yang, X. Zhang, et al., “Consideration of a Credibility Assessment Framework in Model-Informed Drug Development: Potential Application to Physiologically-Based Pharmacokinetic Modeling and Simulation,” *CPT: Pharmacometrics & Systems Pharmacology* 9 (2020): 21–28.

46. J. P. F. Bai, B. J. Schmidt, K. G. Gadkar, et al., “FDA-Industry Scientific Exchange on Assessing Quantitative Systems Pharmacology Models in Clinical Drug Development: A Meeting Report, Summary of Challenges/Gaps, and Future Perspective,” *AAPS Journal* 23 (2021): 60.

47. F. T. Musuamba, I. Skotheim Rusten, R. Lesage, et al., “Scientific and Regulatory Evaluation of Mechanistic In Silico Drug and Disease

Models in Drug Development: Building Model Credibility,” *CPT: Pharmacometrics & Systems Pharmacology* 10 (2021): 804–825.

## Supporting Information

Additional supporting information can be found online in the Supporting Information section.